Living liquid crystals

Shuang Zhou[a,1], Andrey Sokolov[b,1], Oleg D. Lavrentovich[a,2], and Igor S. Aranson[b,c,2]

[a]Liquid Crystal Institute and Chemical Physics Interdisciplinary Program, Kent State University, Kent, OH 44242; [b]Materials Science Division, Argonne National Laboratory, Argonne, IL 60439; and [c]Engineering Sciences and Applied Mathematics, Northwestern University, Evanston, IL 60202

Edited by David A. Weitz, Harvard University, Cambridge, MA, and approved December 12, 2013 (received for review November 22, 2013)

Collective motion of self-propelled organisms or synthetic particles, often termed "active fluid," has attracted enormous attention in the broad scientific community because of its fundamentally nonequilibrium nature. Energy input and interactions among the moving units and the medium lead to complex dynamics. Here, we introduce a class of active matter—living liquid crystals (LLCs)—that combines living swimming bacteria with a lyotropic liquid crystal. The physical properties of LLCs can be controlled by the amount of oxygen available to bacteria, by concentration of ingredients, or by temperature. Our studies reveal a wealth of intriguing dynamic phenomena, caused by the coupling between the activity-triggered flow and long-range orientational order of the medium. Among these are (*i*) nonlinear trajectories of bacterial motion guided by nonuniform director, (*ii*) local melting of the liquid crystal caused by the bacteria-produced shear flows, (*iii*) activity-triggered transition from a nonflowing uniform state into a flowing one-dimensional periodic pattern and its evolution into a turbulent array of topological defects, and (*iv*) birefringence-enabled visualization of microflow generated by the nanometers-thick bacterial flagella. Unlike their isotropic counterpart, the LLCs show collective dynamic effects at very low volume fraction of bacteria, on the order of 0.2%. Our work suggests an unorthodox design concept to control and manipulate the dynamic behavior of soft active matter and opens the door for potential biosensing and biomedical applications.

motile bacteria | self-organization | cromonic liquid crystals

Active matter has recently emerged as an important physical model of living systems that can be described by the methods of nonequilibrium statistical mechanics and hydrodynamics (1–3). Active matter is driven by the internal sources of energy, associated with the self-propelled particles such as bacteria or synthetic swimmers. The interaction of these active particles among themselves and with the medium produces a rich variety of dynamic effects and patterns. Most of the studies deal with active particles embedded into a Newtonian isotropic fluid. In this case the interactions among particles are caused by long-range hydrodynamic and short-range excluded volume effects (4–13). In this work, we conceive a general class of active fluids, termed living liquid crystals (LLCs). The suspending medium is a nontoxic liquid crystal (LC) that supports the activity of self-propelled particles, namely bacteria. At the very same time, the medium imposes long-range anisotropic interactions onto bacteria, thanks to the intrinsic orientational order that persists even when the bacteria are not active. The importance of this system is twofold. Firstly, the bacterial activity modifies the orientational order of the system, by producing well-defined and reproducible patterns with or without topological defects. Secondly, the orientational order of the suspending medium reveals facets of bacterial behavior, allowing one to control trajectories of individual bacteria and to visualize rotation of flagella through birefringence of the host. The LLCs represent an example of a biomechanical system, capable of controlled transduction of stored energy into a systematic movement, which is of critical importance in a variety of applications, from bioinspired micromachines to self-assembled microrobots (14,15). The study of bacterial motion in LCs and non-Newtonian fluids takes us a step closer to realizing in vitro environments that more closely resemble conditions in vivo (16,17).

Results

The concept of LLC is enabled by the recent progress in water-soluble nontoxic chromonic LCs (16–18) and growing expertise in control and manipulation of bacterial suspensions in confined geometries (10–14). Our studies have shown that living bacteria can be transferred to the LC media, and yield highly nontrivial interactions with the molecular ordering of the LC. The experiments are conducted with common swimming bacteria (*Bacillus subtilis)* in lyotropic chromonic (*Materials and Methods*). We examined the simplest nematic phase of the LLC. In the absence of activity, the LLC is a standard nematic characterized by the long-range orientational order described by a unit director $\hat{\mathbf{n}}$ with the property $\hat{\mathbf{n}} = -\hat{\mathbf{n}}$. Its ground state is a uniform director field, $\hat{\mathbf{n}} = \text{const}$. When activity is turned on, the LLC exhibits the onset of large-scale undulations of a nematic director with a characteristic length ξ (see *Results* and *Discussion*) determined by the balance between bacteria activity and anisotropic viscoelasticity of the lyotropic chromonic. The nematic phase of the LLC depends on both the concentration of the mesogenic material and temperature; at low concentrations and/or high temperatures, the material melts into an isotropic fluid. The bacterial-free chromonic LC and the LLC show approximately the same phase diagram in the concentration–temperature coordinates. In an experimental cell, the direction of $\hat{\mathbf{n}}$ is preselected by surface anchoring, namely by a rubbed layer of polyimide coated onto the glass substrates (19) (*Materials and Methods*); this direction is along the x axis, so that the unperturbed director is $\hat{\mathbf{n}}_0 = (1, 0, 0)$.

Significance

We propose a class of active matter, the living liquid crystal (LLC), representing motile rod-shaped bacteria placed in water-based nontoxic liquid crystal. Long-range orientational order of the liquid crystal and the swimming activity of bacteria demonstrate a strong coupling that dramatically alters individual and collective bacterial dynamics. For example, swimming bacteria perturb the orientational order of the liquid crystal or even cause its local melting, making the flagella motion optically visible. Second, self-organized textures emerge from the initial uniform LLC alignment with a characteristic length controlled by a balance between bacteria activity and anisotropic viscoelasticity of liquid crystal. Third, the local liquid crystal orientation controls the direction of motion of bacteria. LLC can lead to valuable biosensoring and biomedical applications.

Author contributions: S.Z., A.S., O.D.L., and I.S.A. designed research; S.Z., A.S., O.D.L., and I.S.A. performed research; S.Z., A.S., O.D.L., and I.S.A. analyzed data; and S.Z., A.S., O.D.L., and I.S.A. wrote the paper.

The authors declare no conflict of interest.

This article is a PNAS Direct Submission.

[1]S.Z. and A.S. contributed equally to this work.

[2]To whom correspondence may be addressed. E-mail: olavrent@kent.edu or aronson@anl.gov.

This article contains supporting information online at www.pnas.org/lookup/suppl/doi:10.1073/pnas.1321926111/-/DCSupplemental.

A typical bacterium has a cylindrical body of length 5–7 μm and diameter 0.7 μm. There are also about 20 helicoidal 10-μm-long flagella filaments attached to the bacterial body. In an active (motile) bacterium, the filaments bundle on one end of the bacterium and rotate, thus powering unidirectional "head-forward" motion. The motility of aerobic bacteria (such as *B. subtilis*) is controlled by the amount of dissolved oxygen (10, 13, 14). When placed in the uniformly aligned LC, the bacteria show a number of intriguing dynamic phenomena that can be attributed to the coupling of the LC structure to an individual bacterium and to the collective effects. Because the individual behavior is pertinent for the understanding of emerging collective motion, we first discuss the dynamics of individual bacteria in relatively thin (of thickness $h = 5$ μm) LLC flat glass cells (Fig. 1).

Because of the rod-like shape of the bacterium, and because of the strong orienting effect of the surface anchoring in a thin LC cell, individual bacteria tend to swim along director $\hat{\mathbf{n}}_0$, in agreement with earlier observations (17, 20). The most striking feature observed in our experiments is that the bacterial flagella, having a diameter of only about 24 nm, produces director perturbations on a scale of micrometers (Fig. 1 *A*–*C*). Birefringence of the LLC makes these perturbations clearly seen under the polarizing microscope (Fig. 1*A*). The texture in Fig. 1*A* observed with de-crossed polarizers reveals periodic dark and bright elongated spots tilted with respect to $\hat{\mathbf{n}}_0$ and caused by the broken chiral symmetry of the director distortions (*SI Text* and Figs. S1–S3). The map of optical retardance in Fig. 1*B*, obtained with a PolScope (*Materials and Methods*) (21), demonstrates that the effective birefringence near the bacterium is reduced compared with the uniform director surrounding.

The pattern of alternating bright and dark spots in the bacterium wake propagates with a wavelength about $d = 2$ μm. At a fixed distance from the body of bacterium, the bright and dark regions alternate with the frequency of about 16 Hz (Fig. 1*C*). The wavelength is determined by the pitch of helical flagella, and the frequency by the flagella rotation rate. We constructed a space–time diagram by stacking a total of 240 consecutive cross-sections along the bacterium's axis in a comoving reference frame from each image (Fig. 1*D*). From the space–time diagram we clearly see propagation of the flagella wave (parallel white lines between 0 and 15 μm) and counterrotation of the bacterial body (dark regions at −5 μm) with a frequency of 2.5 Hz. The ratio of

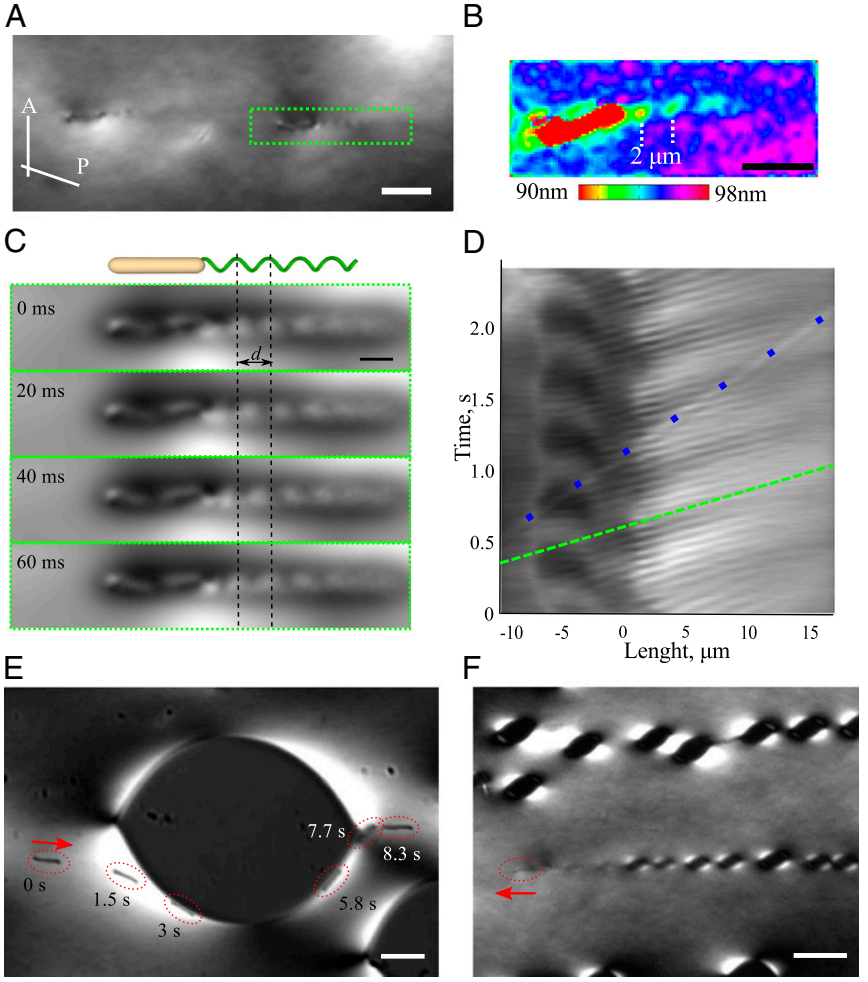

Fig. 1. Distortion of the nematic director detected by optical microscopy. (*A*) Snapshot of swimming bacteria observed under a microscope with slightly de-crossed polarizer (P) and analyzer (A). The bacterium shown in green box swims from right to left. (*B*) Optical retardance pattern around a swimming bacterium; see also Figs. S1–S3. (*C*) Time evolution of the director waves created by rotating flagella in the comoving reference frame. (*D*) Space–time diagram for director waves extracted for the bacterium shown in *C*. A total of 240 cross-sections was extracted from 2.4 s of video. Dashed green line depicts phase velocity of the flagella wave. Dots mark an immobilized dust particle. See also Movies S1 and S2. (*E*) Trajectory of a single bacterium around a tactoid. (*F*) Trace of isotropic tactoids left by a bacterium at temperature about 0.5 °C below the nematic–biphasic transition point. Observations are made under a microscope with slightly de-crossed polarizer (P) and analyzer (A). Scale bar, 5 μm (*A* and *B*); 2 μm (*C*); 10 μm (*E*); and 20 μm (*F*). See Movies S3 and S4.

flagella rotation to the counterrotation of the body is about 7:1, similar to that known for *B. subtilis* under normal conditions [160-Hz flagella rotation and 20-Hz body counterrotation (22)].

Individual behavior of bacteria and its coupling to the orientational order becomes especially interesting as the temperature is increased and the LLC approaches a biphasic region, in which the isotropic and nematic phases coexist. The isotropic regions appear as characteristic "negative tactoids" elongated along the overall director of the surrounding nematic (23, 24). The isotropic tactoids, seen as dark islands in Fig. 1*E*, distort the director around them and change the trajectories of the bacteria. As shown in Fig.1*E*, far away from the tactoid, a bacterium is swimming along a straight line set by the uniform director. In the vicinity of tactoid, the trajectory deviates from the straight line and follows the local distorted director. After a collision with the isotropic–nematic interface, the bacterium follows the curved interface, and finally escapes at the cusp of the tactoid.

Even more strikingly, the bacteria themselves can create isotropic tactoids in their wake if the LLC temperature is close to the biphasic region (Fig. 1*F*). The LLC acts as a miniature "Wilson chamber," in which the isotropic droplets decorate the path of swimming bacteria. The feature underscores the complexity of interplay between velocity fields and the state of orientational order that can involve a number of different mechanisms, such as existence of a nucleation barrier, nonuniform distribution of components between the nematic and isotropic phase, etc. Nucleation of the isotropic phase in Fig. 1*F* implies that the bacterial flows reduce the local degree of orientational order, most probably through disintegration of the chromonic aggregates (18). The fact that bacteria can follow the nematic–isotropic interface and the overall director in the LLC offers numerous design concepts of reconfigurable microfluidic devices for the control and manipulation of bacteria. The desired trajectories of bacterial transport can be engineered by patterned surface

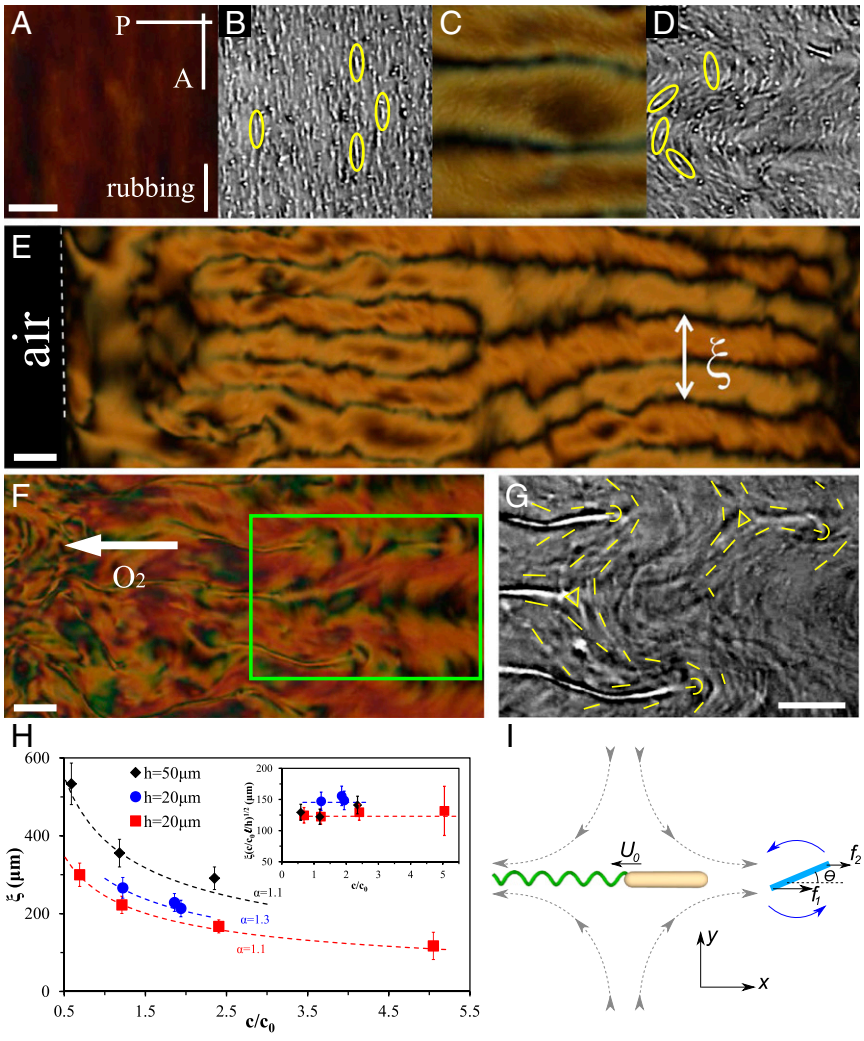

Fig. 2. Emergence of a characteristic length scale in LLCs. (*A* and *B*) LLC with inactive bacteria is at its equilibrium state with the director and bacteria (highlighted by ellipses) aligned uniformly along the rubbing direction; (*C* and *D*) active bacteria produce periodically distorted director. (*E*) Proliferation of stripe pattern in the sample of thickness $h = 20$ μm and for low concentration of bacteria, $c \sim 0.9 \times 10^9$ cells/cm^3. Oxygen permeates from the left-hand side. (*F*) LLC patterns in thicker sample ($h = 50$ μm) and for higher concentration of bacteria, $c \sim 1.6 \times 10^9$ cells/cm^3. White arrow points toward a higher concentration of oxygen. (*G*) Zoomed area in *F* showing nucleating disclinations of strength +1/2 (semicircles) and −1/2 (triangles). Bright dashes visualize bacterial orientation. (*H*) Dependence of characteristic period ξ on c and h; dashed lines depict fit to theoretical prediction $\xi = \sqrt{\frac{K\ h}{c\alpha_0 U_0}}$. (*Inset*) Illustration of collapse of the data into a universal behavior that follows from the theoretical model. (*I*) Director realignment (shown as a rod) caused by the bacterium-generated flow (shown by dashed lines with arrows). See also Movies S5 and S6. Scale bar, 50 μm (*A–D*); 100 μm (*E–G*). Error bars, ±10% standard error of the mean (SEM), except for ±30% SEM at $c/c_0 = 5.05$.

anchoring and by local dynamic heating (for example, with focused laser beams).

Now we discuss collective behavior of LLC emerging at higher concentrations of bacteria. We discovered that a long-range nematic alignment of the LLC is affected by the flow created by the swimming bacteria. The coupling of the orientational order and hydrodynamic flow yields nontrivial dynamic patterns of the director and bacterial orientations (Figs. 2 and 3 and *SI Text*).

The first example, Fig. 2, demonstrates the existence of a characteristic spatial length scale ξ in LLCs that sets this nonequilibrium system apart from standard equilibrium LCs. The LLC is confined between two glass plates that fix $\hat{\mathbf{n}}_0 = (1, 0, 0)$ along the rubbing direction. In the samples with inactive bacteria the steady state is uniform, $\hat{\mathbf{n}} = \hat{\mathbf{n}}_0 = \text{const}$, and the immobilized bacteria are aligned along the same direction (Fig. 2 *A* and *B*). In chambers with active bacteria, supported by the influx of oxygen through the air–LLC interface (on the left-hand side in Fig. 2*E*), the uniform state becomes unstable and develops a stripe pattern with periodic bend-like deviations of $\hat{\mathbf{n}}$ from $\hat{\mathbf{n}}_0$ (Fig. 2 *C*–*E*). The swimming bacteria are aligned along the local director $\hat{\mathbf{n}}$ (Fig. 2*D*). Because the oxygen permeates the LLC from the open side of the channel, its concentration is highest at the air–LC interface; accordingly, the stripes appear first near the air–LLC interface. The period ξ of stripes increases with the increase of the distance from the air–LLC interface as the amount of oxygen and the bacterial activity decrease. Fig. 2*H* shows that ξ increases with the decrease in the concentration c of bacteria and the increase in the chamber thickness h. The data in Fig. 2*H* are collected for different samples in which the velocity of bacteria was similar (8 ± 3 μm/s), as established by a particle-tracking velocimetry; the concentration is normalized by the concentration $c_0 \sim 8 \times 10^8$ cells/cm^3 of the stationary growth phase.

As time evolves, in the regions with the highest bacterial activity, near the open edge, the stripe pattern becomes unstable against nucleation of pairs of ±1/2 disclinations (Fig. 2 *F* and *G*). Remarkably, the pattern-forming instabilities occurring here have no direct analog for bacterial suspensions in Newtonian fluids or for bacteria-free pure LCs. The concentration of bacteria in our experiments (close to 0.2% of volume fraction) is about 1/10 of that needed for the onset of collective swimming in Newtonian liquids [about 10^{10} cells/cm^3 (10)].

Fig. 3 illustrates the profound effect of bacterial activity on spatiotemporal patterns in a sessile drop of LLCs (10, 25) in which there is no preferred director orientation in the plane of film. Bacterial activity generates persistently rearranging bacterial and director patterns with ±1/2 disclinations that nucleate and annihilate in pairs, similarly to the recent experiments on active microtubule bundles (4) (Fig. 3*A*). The characteristic spatial scale of the pattern, determined as an average distance between the disclination cores, is in the range of 150–200 μm, of the same order of magnitude as ξ in the stripe pattern in strongly anchored sample. The fluid flow typically encircles disclination pairs (Fig. 3 *B*–*D*).

Discussion

Emergence of a characteristic length scale ξ in LLCs, either as a period of the stripe pattern in Fig. 2 or as a characteristic separation of disclinations in Fig. 3, is caused by the balance of director-mediated elasticity and bacteria-generated flow (Fig. 2*I*). Because no net force is applied to a self-propelled object, a swimming bacterium represents a moving negative hydrodynamic force dipole of the strength U_0 ("pusher"), as it produces two outward fluid streams coaxial with the bacterial body (26). The strength of the dipole (of a dimension of torque or energy) is of the order of 1 pN μm (27). In the approximation of nearly parallel orientation of the bacterium and the local director $\hat{\mathbf{n}}$, the bacteria-induced streams (Fig. 2*I*) impose a reorienting torque $\sim\alpha(h)cU_0\theta$, where $\alpha(h)$ is a dimensionless factor that describes the flow strength and depends on the cell thickness h; c is the concentration of bacteria, and θ is the angle between local orientation of bacteria and $\hat{\mathbf{n}}$. Similar torques caused by shear flow are well known in the physics of LCs (24); *SI Text* and Fig. S3. Mass conservation yields an estimate $\alpha = \alpha_0 l/h$, where constant $\alpha_0 \sim O(1)$, and l is the length of a bacterium. It implies that the channel's thickness reduction increases the flow because the bacteria pump the same amount of liquid. The local bacterium-induced reorienting hydrodynamic torque is opposed by the restoring elastic torque $\sim K\frac{\partial^2\theta}{\partial x^2}$; K is an average Frank elastic constant of the LC. In the case of a very thin layer confined between two plates with strong surface anchoring, the strongest elastic torque $K\frac{\partial^2\theta}{\partial z^2}$ will be associated with the twist deformation along the vertical z axis. However, because the elastic constant for twist is an order of magnitude smaller than the splay and bend constants (28), the restoring torque in relatively thick (20- and 50-μm) samples is caused mainly by in-plane distortions. By balancing the elastic and bacterial torques, $\partial^2\theta/\partial x^2 = \theta/\xi^2$, one

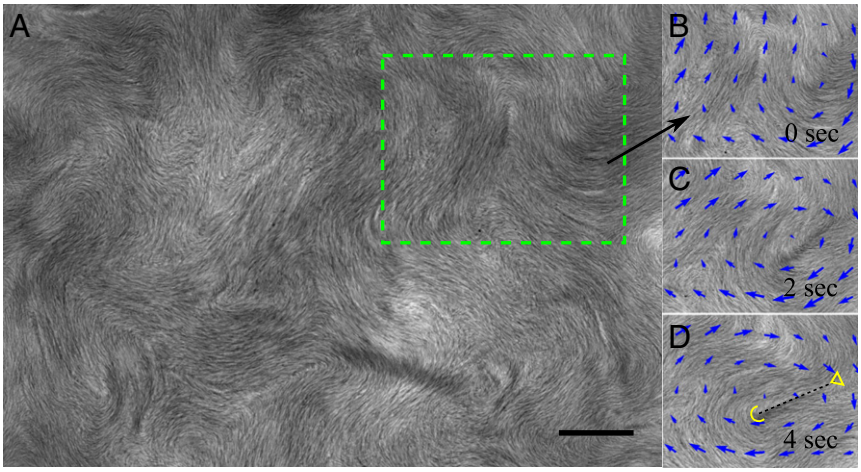

Fig. 3. LLC in sessile drop. (*A*) Texture with multiple disclination pairs; green rectangle indicates the region shown in *B*, *C*, and *D*. Bacteria are aligned along the local nematic director, as revealed by the fine stripes. Scale bar, 30 μm; no polarizers. See also Movie S7. (*B*, *C*, and *D*) LLC texture with −1/2 and +1/2 disclinations and the pattern of local flow velocity (blue arrows) determined by particle-image velocimetry. The flow typically encircles the close pair of defects.

defines a "bacterial coherence length" $\xi = \sqrt{\frac{K\,h}{\alpha_0 l\, c U_0}}$ (somewhat similar arguments for the characteristic length of bending instability in active nematics were suggested in ref. 2). This expression fits the experimental data on the periodicity of stripe patterns for different concentrations of bacteria c and thicknesses h remarkably well with a choice of $\alpha_0 \sim 1$ (Fig. 2*H*). A simple phenomenological theory shows that competition between bacteria-generated hydrodynamic torque and restoring elastic torque yields nontrivial pattern-forming instability (*SI Text* and Fig. S4).

The experiments in Figs. 2 and 3 clarify the rich sequence of instabilities by which the activity of bacteria transforms the initial nonflowing homogeneous uniform steady state in Fig. 2 *A* and *B* into the state of self-sustained active fluid turbulence (Fig. 3). The first step is through appearance of the periodic director undulations with a characteristic length scale ξ (Fig. 2 *C*–*E*). The period becomes shorter as the activity increases (Fig. 2*H*). Further escalation of the activity causes a qualitative transformation, namely nucleation of defect pairs, Fig. 2 *F* and *G*. Note that the axis connecting the cores of +1/2 and −1/2 disclinations in the pair and the local director $\hat{\mathbf{n}}$ along this axis are perpendicular to the original director $\hat{\mathbf{n}}_0$ (Fig. 2*G*). Once the system overcomes the stabilizing action of surface anchoring, as in Fig. 3, the dynamic array of moving defects forms a globally isotropic state in which the director $\hat{\mathbf{n}}$ is defined only locally (somewhat similar dynamic behavior was observed in simulations of an "active nematic" in refs. 29, 30). The final state, Fig. 3, is an example of "active fluid" turbulence at vanishing Reynolds number (10, 25), which in our case is on the order of 10^{-5}.

In conclusion, LLC demonstrates a wealth of phenomena not observed for either suspension of bacteria in a Newtonian fluid or in passive ordered fluid (see Fig. S5). The concept of a characteristic length ξ, contrasting the elastic response of orientationally ordered medium and the activity of microswimmers, may also be useful for understanding hierarchy of spatial scales in other active matter systems (6–11). Our studies were focused on the simplest nematic LLC. However, more complex LLCs can be explored as well, for example, smectics and cholesteric LCs with controlled chirality. Exploration of LLCs may have intriguing applications in various fields. Our biomechanical system may provide the basis for devices with unique functionalities, including specific responses to chemical agents, toxins, or photons. Swimming bacteria can also serve as autonomous "microprobes" for the properties of LCs. Unlike passive microprobes (31), swimming bacteria introduce local perturbations of the LC molecular order both in terms of the director and the degree of order, and thus provide unique information on the mesostructure of the material. In turn, LC medium provides valuable optically accessible information on the intricate submicrometer structure of bacteria-generated microflow that deserves further investigation.

Materials and Methods

Bacteria. Experiments were conducted with the strain 1085 of *B. subtilis*, rod-shaped bacterium 5–7 μm long and 0.7 μm in diameter. The bacteria were initially grown on LB agar plates, then transferred to a Terrific Broth liquid medium (Sigma T5574) and grown in shaking incubator at temperature 35 °C for 10–12 h. To increase resistance to oxygen starvation, the bacteria are grown in sealed vials under microaerobic conditions (10). We monitored the concentration of bacteria by the measurement of the optical scattering of the growth media. The bacteria at the end of their exponential growth stage were extracted and washed. The growth medium was separated from the bacteria and removed as completely as possible by centrifugation.

LLC Preparation. Chromonic lyotropic LC material disodium cromoglycate (DSCG) purchased from Spectrum Chemicals, 98% purity, was dissolved in Terrific Broth at 16 wt %. This solution was added to the concentrated bacteria obtained as described above. The resulting LLC was mixed by stirring with a clean toothpick and then in a vortex mixer at 3,000 rpm. The LLC mixture was injected (by pressure gradient) into a flat cell made from two square glass plates (10 × 10 mm) separated by spacers. Two interior surfaces were pretreated with polyimide SE7511 and rubbed with velvet cloth to provide a uniform planar alignment of the LLC. The cell was sealed with high vacuum grease (Dow Corning) to prevent water evaporation. The temperature shift of the LC phase diagrams during several hours of the experiments is less than 1 °C and thus does not affect the data presented. The observations were started immediately after the sealed cells were placed in a heating stage (Linkam PE94) at 25 °C. For the used lyotropic LC, the average value of the splay and bend elastic constants is K = 10–12 pN (28); the average viscosity $\eta \sim 10$ kg/(m s) as determined in an experiment with director relaxation in cells with magnetically induced director distortions (Frederiks effect) (24, 28).

Videomicroscopy. An inverted microscope Olympus IX71 with a motorized stage, mounted on a piezoelectric insolation platform Herzan TS-150, and a Prosilica GX 1660 camera (resolution of 1,600 × 1,200) were used to record motion of individual bacteria in thin cells. Images were acquired with the frame rate up to 100 frames/s, at 60× magnification, oil-immersion objective, in cross-polarized light. Color camera with the resolution 1,280 × 1,024 and the frame rate 10 frames/s and 2–20× magnifications were used to acquire large-scale patterns of collective motion. The acquired images were processed in MATLAB.

PolScope Microscopy. The LLC textures were examined by a polarizing microscope (Nikon E600) equipped with Cambridge Research Incorporation Abrio LC-PolScope package. The LC PolScope uses a monochromatic illumination at 546 nm and maps optical retardance $\Gamma(x,y)$ in the range (0–273) nm and orientation of the slow axis (21). For tangentially anchored LLC, $\Gamma = |n_e - n_0|h$, where n_e and n_o are the extraordinary and ordinary refractive indices, respectively, and h is the cell thickness. For DSCG, optical birefringence is negative, $n_e - n_0 \approx -0.02$ (18). The slow axis is thus perpendicular to the optic axis and to $\hat{\mathbf{n}}$. The PolScope was set up to map the local orientation $\hat{\mathbf{n}}(x,y)$ (Fig. S2*B*).

ACKNOWLEDGMENTS. The research of A.S. and I.S.A. was supported by the US Department of Energy, Office of Basic Energy Sciences, Division of Materials Science and Engineering, under Contract DE AC02-06CH11357. O.D.L. and S.Z. were supported by National Science Foundation Grant DMR 1104850.

1. Vicsek T, Zafeiris A (2012) Collective motion. *Phys Rep* 517(3-4):71–140.
2. Ramaswamy S (2010) The mechanics and statistics of active matter. *Ann Rev Condens Matter Phys* 1(1):323–345.
3. Marchetti MC, et al. (2013) Hydrodynamics of soft active matter. *Rev Mod Phys* 85(3): 1143–1189.
4. Sanchez T, Chen DTN, DeCamp SJ, Heymann M, Dogic Z (2012) Spontaneous motion in hierarchically assembled active matter. *Nature* 491(7424):431–434.
5. Sumino Y, et al. (2012) Large-scale vortex lattice emerging from collectively moving microtubules. *Nature* 483(7390):448–452.
6. Palacci J, Sacanna S, Steinberg AP, Pine DJ, Chaikin PM (2013) Living crystals of light-activated colloidal surfers. *Science* 339(6122):936–940.
7. Schaller V, Weber C, Semmrich C, Frey E, Bausch AR (2010) Polar patterns of driven filaments. *Nature* 467(7311):73–77.
8. Zhang HP, Be'er A, Florin EL, Swinney HL (2010) Collective motion and density fluctuations in bacterial colonies. *Proc Natl Acad Sci USA* 107(31):13626–13630.
9. Schwarz-Linek J, et al. (2012) Phase separation and rotor self-assembly in active particle suspensions. *Proc Natl Acad Sci USA* 109(11):4052–4057.
10. Sokolov A, Aranson IS (2012) Physical properties of collective motion in suspensions of bacteria. *Phys Rev Lett* 109(24):248109.
11. Wensink HH, et al. (2012) Meso-scale turbulence in living fluids. *Proc Natl Acad Sci USA* 109(36):14308–14313.
12. Gachelin J, et al. (2013) Non-Newtonian viscosity of Escherichia coli suspensions. *Phys Rev Lett* 110(26):268103.
13. Dunkel J, et al. (2013) Fluid dynamics of bacterial turbulence. *Phys Rev Lett* 110(22): 228102.
14. Sokolov A, Apodaca MM, Grzybowski BA, Aranson IS (2010) Swimming bacteria power microscopic gears. *Proc Natl Acad Sci USA* 107(3):969–974.
15. Snezhko A, Aranson IS (2011) Magnetic manipulation of self-assembled colloidal asters. *Nat Mater* 10(9):698–703.
16. Woolverton CJ, Gustely E, Li L, Lavrentovich OD (2005) Liquid crystal effects on bacterial viability. *Liquid Crystals* 32(4):417–423.
17. Mushenheim PC, et al. (2014) Dynamic self-assembly of motile bacteria in liquid crystals. *Soft Matter* 10(1):88–95.
18. Park HS, Lavrentovich OD (2012) *Liquid Crystals Beyond Displays: Chemistry, Physics, and Applications*, ed Li Q (Wiley, New Jersey), pp 449–484.

19. Nastishin YA, et al. (2005) Optical characterization of the nematic lyotropic chromonic liquid crystals: Light absorption, birefringence, and scalar order parameter. *Phys Rev E Stat Nonlin Soft Matter Phys* 72(4 Pt 1):041711.
20. Kumar A, Galstian T, Pattanayek SK, Rainville S (2013) The motility of bacteria in an anisotropic liquid environment. *Mol Cryst Liq Cryst (Phila Pa)* 574(1):33–39.
21. Shribak M, Oldenbourg R (2003) Techniques for fast and sensitive measurements of two-dimensional birefringence distributions. *Appl Opt* 42(16):3009–3017.
22. Dewenter L, Alpmann C, Woerdemann M, Denz C (2012) Video-based analysis of the rotational behaviour of rod-shaped, self-propelled bacteria in holographic optical tweezers. *Proc SPIE* 8427:84270N.
23. Kim Y-K, Shiyanovskii SV, Lavrentovich OD (2013) Morphogenesis of defects and tactoids during isotropic-nematic phase transition in self-assembled lyotropic chromonic liquid crystals. *J Phys Condens Matter* 25(40):404202.
24. Kleman M, Lavrentovich OD (2003) *Soft Matter Physics: An Introduction* (Springer, New York), pp 135–218.
25. Dombrowski C, Cisneros L, Chatkaew S, Goldstein RE, Kessler JO (2004) Self-concentration and large-scale coherence in bacterial dynamics. *Phys Rev Lett* 93(9):098103.
26. Kim S, Karrila S (2005) *Microhydrodynamics: Principles and Selected Applications* (Dover, New York), pp 107–162.
27. Drescher K, Dunkel J, Cisneros LH, Ganguly S, Goldstein RE (2011) Fluid dynamics and noise in bacterial cell-cell and cell-surface scattering. *Proc Natl Acad Sci USA* 108(27): 10940–10945.
28. Zhou S, et al. (2012) Elasticity of lyotropic chromonic liquid crystals probed by director reorientation in a magnetic field. *Phys Rev Lett* 109(3):037801.
29. Giomi L, Bowick MJ, Ma X, Marchetti MC (2013) Defect annihilation and proliferation in active nematics. *Phys Rev Lett* 110(22):228101.
30. Thampi SP, Golestanian R, Yeomans JM (2013) Velocity correlations in an active nematic. *Phys Rev Lett* 111(11):118101.
31. De Luca A, et al. (2008) Optical nanotomography of anisotropic fluids. *Nat Phys* 4(11):869–872.